



## Research article

# Synthesis, characterization and adsorption optimization of bimetallic La–Zn metal organic framework for removal of 2,4-dichlorophenylacetic acid

Omaymah Alaysuy<sup>a</sup>, Meshari M. Aljohani<sup>a</sup>, Kholood Alkhamis<sup>a</sup>, Nada M. Alatawi<sup>a</sup>, Awatif R.Z. Almotairy<sup>b</sup>, Khulood A. Abu Al-Ola<sup>c</sup>, Abdelrahman S. Khder<sup>d,e</sup>, Nashwa M. El-Metwaly<sup>d,e,\*</sup>

<sup>a</sup> Department of Chemistry, College of Science, University of Tabuk, 71474, Tabuk, Saudi Arabia

<sup>b</sup> Department of Chemistry, Faculty of Science, Taibah University, Yanbu, 30799, Saudi Arabia

<sup>c</sup> Department of Chemistry, College of Science, Taibah University, 30002, Al-Madinah Al-Munawarah, Saudi Arabia

<sup>d</sup> Department of Chemistry, Faculty of Applied Sciences, Umm Al-Qura University, Makkah, Saudi Arabia

<sup>e</sup> Department of Chemistry, Faculty of Science, Mansoura University, El-Gomhoria Street 35516, Egypt



## ARTICLE INFO

## Keywords:

La/Zn-MOF  
2,4-Dichlorophenylacetic acid  
Box-behnken design  
Adsorption  
Interaction mechanism

## ABSTRACT

To eliminate the hazardous pesticide 2,4-dichlorophenylacetic acid (2,4-D) through aqueous solutions, stacked nanorods known as hetero bimetallic organic frameworks (MOFs) of 2-methyl imidazole based on lanthanum and zinc are created. The research's convincing discoveries displayed that La/Zn-MOF is an actual adsorbent for the removal of 2,4-D through aqueous solutions. The La/Zn-MOF was investigated using a variability of techniques, with scanning electron microscope (SEM), powered X-ray diffraction (PXRD), and Brunauer-Emmett-Teller (BET) investigation. La/Zn-MOF has a significant pore capacity of 1.04 cm<sup>3</sup>/g and a comparatively large surface area of 897.69 m<sup>2</sup>/g. Our findings, which are quite intriguing, demonstrate that adsorption behavior is pointedly wedged by variations in pH. A pH 6 dose of 0.02 g was shown to be the optimal setting for the greatest capacity for adsorption. Because adsorption is an endothermic process, temperature variations affect its capability. The adsorption method was fit both isothermally and kinetically using the Langmuir isotherm classical. It was created that the entire process made use of a chemisorption mechanism. Solution pH, temperature, adsorbent dosage, and time were all improved using the Box-Behnken design (BBD) and Response Surface Methodology (RSM). We were able to accurately calculate the values of  $\Delta H^\circ$ ,  $\Delta S^\circ$ , and  $\Delta G^\circ$  for 2,4-D by following the guidelines. These results demonstrated the spontaneous and endothermic character of the adsorption procedure employing La/Zn-MOF as an adsorbent. Adsorption-desorption cycles can be carried out up to five times. With the synthesized La/Zn-MOF adsorbent due to its exceptional reusability. Many processes, such  $\pi$ - $\pi$  interaction, pore filling, H-bonding, or electrostatic contact, were postulated to explain the connection between La/Zn-MOF and 2,4-D after extra research to appreciate well the link was conducted. This is the first study to demonstrate the effectiveness of utilizing La/Zn-MOF as an adsorbent to eliminate 2,4-D from wastewater models. The results display that a pH of 6 is required to achieve the maximal 2,4-D adsorption capability on La/Zn-MOF, which is 307.5 mg/g.

\* Corresponding author. Department of Chemistry, Faculty of Applied Sciences, Umm Al-Qura University, Makkah, Saudi Arabia.  
E-mail address: [n\\_elmetwaly00@yahoo.com](mailto:n_elmetwaly00@yahoo.com) (N.M. El-Metwaly).

<https://doi.org/10.1016/j.heliyon.2024.e28622>

Received 4 September 2023; Received in revised form 20 March 2024; Accepted 21 March 2024

Available online 26 March 2024

2405-8440/© 2024 The Authors. Published by Elsevier Ltd. This is an open access article under the CC BY-NC-ND license (<http://creativecommons.org/licenses/by-nc-nd/4.0/>).

## 1. Introduction

Pesticides in wastewater pose serious intimidation to the situation, human health, and aquatic ecosystems. They contaminate water bodies, disrupting ecosystems, harming non-target organisms, and contributing to the development of pesticide-resistant pests. Ingestion of contaminated water can lead to acute poisonings, chronic health issues, and increased risks of cancer. To address these concerns, it is essential to implement effective wastewater treatment, promote sustainable agriculture, reduce pesticide use, and enforce stringent regulations to safeguard both the environment and human health [1]. 2,4-D, classified as a herbicide for broadleaf weed control, belongs to a broader spectrum of pesticides designed for various purposes [2]. Herbicides such as glyphosate, atrazine, dicamba, and paraquat are utilized for targeted or widespread plant management. Insecticides, including malathion, chlorpyrifos, imidacloprid, and permethrin, serve to combat insect infestations, while fungicides like captan, mancozeb, thiophanate-methyl, and copper-based formulations prevent or treat fungal diseases in crops. Rodenticides, such as warfarin, bromadiolone, diphacinone, and brodifacoum, find application in rodent control [3]. Nematicides, like fenamiphos, carbofuran, and fosthiazate, address nematode-related concerns in agricultural settings. Molluscicides such as metaldehyde and iron phosphate are commonly employed to manage snails and slugs. Adhering to established guidelines and guidelines is imperative to diminish potential adverse environmental and human health influences resulting from the use of these pesticides [4].

Several methods exist for removing pesticides from wastewater, and the choice depends on factors like pesticide types, concentrations, and wastewater characteristics [5]. Common techniques include activated carbon adsorption, where carbon removes pesticides by adsorption; biological treatment, using microorganisms for biodegradation; chemical oxidation, breaking down pesticides with strong oxidants; membrane filtration, utilizing semipermeable membranes like RO and NF; chemical coagulation/flocculation, forming clumps for removal; and adsorbent materials like zeolites and activated alumina [6]. The effectiveness varies, so a combination of processes may be needed, with regular monitoring and maintenance essential for consistent pesticide removal [7].

Pesticides present in wastewater pose significant threats to the environment, human health, and aquatic life [8]. Utilizing adsorbents like activated carbon proves effective in collecting and retaining pesticide molecules due to their extensive surface area besides high adsorption capacity. This results in efficient removal, even at low concentrations. Key advantages of adsorption techniques include broad applicability to various pesticide classes, such as herbicides, insecticides, and fungicides, making it suitable for diverse wastewater treatment scenarios. Additionally, adsorption can be discerning, aiming at specific pesticides although sparing additional water constituents [9]. Moreover, the regenerability of adsorbents allows for their multiple reuses, reducing overall pesticide removal costs. The regeneration process involves desorbing pesticides from the adsorbent surface, often through thermal treatment or chemical elution [10,11].

Pesticides in wastewater pose significant risks to the environment, human health, and aquatic life. Like activated carbon, adsorbents efficiently capture pesticide molecules owing to their large surface area and high adsorption capacity, ensuring effective removal even at low concentrations [12]. The versatility of adsorption techniques makes them applicable to a wide range of pesticide compounds, including herbicides, insecticides, and fungicides, providing a suitable option for diverse wastewater treatment scenarios [13]. Additionally, adsorption allows for selective removal, targeting specific pesticide compounds while sparing other water constituents, achieved through the choice of adsorbents with specific affinity towards the target pesticides. Furthermore, the regenerability of adsorbents enables multiple reuses, reducing the overall cost of pesticide removal. Regeneration involves desorbing pesticides from the adsorbent surface, typically through processes like thermal treatment or chemical elution [14]. The efficient and cost-effective use of adsorbents over an extended period makes them a favorable option for pesticide removal [15]. Adsorption techniques seamlessly integrate into existing wastewater treatment systems, whether in fixed-bed columns, as powdered additives, or in combination with other processes like biological treatment or membrane filtration. This adaptability enables optimization based on specific site requirements. Beyond pesticides, adsorption techniques effectively remove various organic micropollutants, including pharmaceuticals, personal care products, and industrial chemicals present in wastewater, offering a versatile solution for multiple pollutant classes [16, 17]. Recognized for its environmental compatibility, adsorption is considered eco-friendly, with adsorbents derived from renewable resources or waste materials, minimizing production-related environmental impacts [18]. Additionally, the adsorption process avoids generating harmful byproducts or residuals, ensuring no adverse belongings on the environment or human health. Overall, the numerous advantages of adsorption techniques establish them as a reliable and effective choice for pesticide removal in wastewater treatment, contributing to safeguarding water resources and mitigating potential negative impacts from pesticide contamination [19, 20].

The use of bimetallic metal-organic frameworks (MOFs) for 2,4-D removal since wastewater is a promising approach. These hybrid materials, composed of metal ions coordinated with organic ligands, offer higher adsorption capacities and synergistic effects compared to traditional adsorbents. The incorporation of two different metal ions in the MOF structure creates additional adsorption sites, enhancing the overall surface area for more efficient pesticide removal [21]. Bimetallic metal-organic frameworks (MOFs) offer enhanced interactions with pesticide molecules, improving adsorption efficiency and selectivity for 2,4-D [22]. Their tunable properties enable customization for optimal adsorption by selecting different metal ions and ligands. Regenerable and cost-effective, bimetallic MOFs can be reused multiple times [23]. They exhibit selective adsorption, removing 2,4-D while sparing other water constituents, reducing the need for extra separation steps. Considered environmentally friendly, these MOFs can be synthesized sustainably, contributing to a reduction in pesticide release [24,25]. Although still emerging, ongoing research suggests the potential of bimetallic MOFs as a promising solution for efficient and selective 2,4-D removal from wastewater [26].

This investigation introduces a newly developed bimetallic organic framework (La/Zn-MOF) designed and characterized specifically for the effective elimination of 2,4-dichlorophenylacetic acid (2,4-D) from water. The La/Zn-MOF showcases a considerable

surface area and a high pore volume, enhancing its ability to adsorb contaminants. The study systematically observes the influence of several influences, including pH, temperature, adsorbent dosage and time, on the adsorption development. The outcomes affirm that the method is endothermic, chemisorptive, and spontaneous, as corroborated by thermodynamic limitations. In summary, this research proposes a favorable method for the effective elimination of 2,4-D from wastewater through the utilization of the La/Zn-MOF.

## 2. Materials and techniques

### 2.1. Resources and instruments

The chemicals Lanthanum nitrate hexahydrate, Zinc nitrate hexahydrate, 2-methylimidazole (Hmim), *N,N*-dimethylformamide, hydrochloric acid, sodium hydroxide, sulfuric acid, ethanol, methanol, and deionized water were obtained from reputable suppliers such as Sigma Aldrich (USA), Duksan Reagents (Korea), and Samchun Pure Chemicals (Korea). These substances were of analytical reagent grades and used with no any additional refining (other details were written in the Supporting material).

### 2.2. Synthesis of La/Zn-MOF

The Lanthanum/Zinc-Metal Organic Framework (La/Zn-MOF) was manufactured using a one-step solvothermal method, succeeding the procedure outlined. In a 20 mL volume of DMF, 4.0 mmol of 2-methylimidazole and 4.0 mmol of a combination of Zn (NO<sub>3</sub>)<sub>2</sub> and La(NO<sub>3</sub>)<sub>3</sub> were separately dissolved while stirring constantly for 30 min. Both solutions were then combined and put into a 100 mL Teflon-lined autoclave. The solvothermal reaction was directed for 20 h at a temperature of 160 °C, followed by cooling to ambient temperature [27,28]. The MOF powders that had accumulated at the bottom of the autoclave reactor were extracted using in the order: DMF, DI water, and ethanol. Overnight, 70 °C was used to dry the MOF powders.

### 2.3. Elimination and batch studies of 2,4-D using La/Zn-MOF

100 mg/L stock solutions of 2,4-D were created. The stock solutions were diluted to achieve the concentration required for the adsorption experiment. The adsorption investigations employed the 2,4-D solution and a 50 mL glass bottle. Through a steady shaking speed of 200 rpm, all reaction flasks swirled for 4 h. Several influencing parameters, including starting pH (2.0–12.0), adsorbent quantity (0.02–0.25 g), adsorption contact time (5–100 min), and temperature (20–45 °C), were examined to achieve the best adsorption conditions. Dropwise additions of dilute solutions of NaOH or HCl were used to change the pH values of the pollutant solution. In 25 mL of solutions containing concentrations of 2,4-D extending from  $8.33 \times 10^{-3}$  to  $1.7 \times 10^{-3}$  mmol/L, 0.02 g of La/Zn-MOF was added for the kinetic experiments. The starting 2,4-D concentration for the thermodynamic experiments was  $1.46 \times 10^{-3}$  mmol/L. The temperature range used for the adsorption of isotherms was 20–45 °C. Tables S1 and S2 contain a list of the detailed information limits for the models used in sorption kinetics, isotherms, and thermodynamics, while Table S3 summarizes a list of abbreviations [29].

La/Zn-MOF (0.02 g) was introduced to 25 mL of 2,4-D solution ( $1.46 \times 10^{-3}$  mmol/L) for 100 min of adsorption for the adsorption-desorption cycle. To remove the adsorbed 2,4-D on La/Zn-MOF, the adsorbed adsorbent was subsequently treated with 25 mL of NaOH (0.1 mol/L) for 2 h. After that, to eliminate excess NaOH, La/Zn-MOF was filtered, numerous times rinsed by deionized water, and then vacuum-dried in preparation for the subsequent adsorption cycle. This adsorbent was used in five separate adsorption-desorption cycle studies. Using an ultraviolet spectrophotometer, the amount of 2,4-D in each cycle's eluate was measured. The concentration of 2,4-D residue was determined by an ultraviolet (UV) spectrophotometer (U-3900, HITACHI, Japan) by calculating the absorbance at the wavelength of maximum absorption ( $\lambda_{\max}$ ) of 283 nm [30,31]. The quantity of 2,4-D residue adsorbed onto the La/Zn-MOF material was calculated by subtracting the original concentration ( $C_0$ ) from the equilibrium concentration ( $C_e$ ). The adsorption capacity ( $q_e$ ) and elimination rate (%) can be determined using the following formulas Eq. 1 and 2:

$$\%R = \frac{(C_0 - C_t)}{C_0} \times 100 \quad (1)$$

$$q_e = \frac{(C_0 - C_e)V}{M} \quad (2)$$

In the equations,  $C_0$  represents the original concentration of 2,4-D,  $C_e$  signifies the equilibrium concentration,  $V$  denotes the solution volume, and  $m$  signifies the mass of the La/Zn-MOF material. These equations enable the assessment of the adsorption capacity and the efficiency of 2,4-D elimination achieved by the La/Zn-MOF material.

### 2.4. Experimental design

Response Surface Methodology (RSM) is a helpful technique for objectively determining the best ways to combine different components to get the best results. Within this process, the Box-Behnken design (BBD) stands out as a specific set of techniques utilized. The Design Expert Version 13 program is where these fitness data were taken from Ref. [32]. Employing mathematical models, the BBD encompasses parameters ranging from first to second order, produced from four-level incomplete factorial designs. To illustrate this

approach, we will construct a scenario in which the objective is to maximize adsorption capacity following three distinct factors: temperature, pH, and time. As a result, studies were accepted out at three different levels: 1, 0, and +1. In the end, RSM gives us the tools to achieve success by offering guidance on how to create the best possible solution for our problem [33,34].

### 3. Results and discussion

#### 3.1. Description of La/Zn-MOF

##### 3.1.1. Powered X-ray diffraction patterns (PXRD)

La/Zn-proposed MOF's structure was determined using PXRD [27]. The stability of the La/Zn-structural MOF was examined by PXRD. The PXRD patterns of the La/Zn-MOF in the  $5^{\circ}$ - $80^{\circ}$  scan range are demonstrated in Fig. 1. The powered X-ray diffraction (PXRD) analysis of the La/Zn-MOF material showed distinct and well-defined peaks at precise  $2\theta$  values. These peaks were observed at  $16.56^{\circ}$ ,  $28.85^{\circ}$ ,  $31.84^{\circ}$ ,  $33.42^{\circ}$ ,  $44.68^{\circ}$ ,  $51.05^{\circ}$ ,  $56.67^{\circ}$ ,  $62.37^{\circ}$ ,  $67.98^{\circ}$ , and  $70.10^{\circ}$ . The presence of these strong and sharp peaks suggests that the La/Zn-MOF material possesses a high level of crystallinity. The surface association of Hmim anions and Sn ions enabled the degree of crystallinity of La/Zn-high MOF. According to Fig. 1, the manufactured La/Zn-MOF material displayed intense crystalline peaks at  $2\theta$  values that were lower than  $16.56^{\circ}$  [35,36]. Using Foolproof and Check Cell software, computations were executed to ascertain the crystal structure of the MOF system containing La and Zn [37]. The outcome pointed to a monoclinic crystal arrangement in the P421C space group. The calculated parameters unveiled the crystal dimensions:  $a = 6.902 \text{ \AA}$ ,  $b = 8.6 \text{ \AA}$ ,  $c = 6.7 \text{ \AA}$ ,  $\alpha = 90^{\circ}$ ,  $\beta = 115.79^{\circ}$ ,  $\gamma = 90^{\circ}$ . Table 1 illustrates the Miller indices (hkl) and interplanar spacing ( $d_{hkl}$ ) for La/Zn-MOF. Notably, even post-adsorption, the La/Zn-MOF nanospheres retained their diffraction peaks. This suggests the crystal structure's impressive resilience [38,39].

##### 3.1.2. Brunauer-Emmett-Teller surface area (BET)

The porosity and surface area characteristics of La/Zn-MOF were evaluated through the BET procedure at 77 K, which entails measuring the samples' nitrogen adsorption-desorption isotherms. Before conducting the measurements, the prepared sample underwent a degassing process under a nitrogen atmosphere at  $150^{\circ}\text{C}$  for 4 h. Further analysis of the sample's surface area and pore size distribution was accomplished utilizing the NLDFT (non-local density functional theory) approach in conjunction with the Brunauer-Emmett-Teller (BET) equation [40,41]. The outcomes of the BET measurements are revealed in Fig. 2. The  $\text{N}_2$  adsorption-desorption process has reversible type III isotherms for the produced La/Zn-MOF [42]. The surface covering of a gas on a solid medium gradually increases with increasing pressure until it reaches a plateau or saturation point in type 3 adsorption. In this instance, the surface of the material is covered by a monolayer of the adsorbed gas molecules, on top of which more layers develop. Typically, the adsorption isotherm has a steep beginning slope that gradually slopes upward until it approaches the saturation point. The adsorbed gas molecules are released from the material's surface during type 3 desorption as the pressure is decreased. Desorption happens gradually and displays a hysteresis loop in the desorption isotherm, just as adsorption [43]. The capillary condensation that occurs within the structure of porous materials, where the adsorbed gas remains trapped in the pores even when the external pressure is lowered, is what causes the hysteresis loop to form. The amount of desorbed gas gradually decreases until it reaches a specific pressure, at which point the desorption process speeds up. A continuous, S-shaped curve is what distinguishes this kind of hysteresis loop. The adsorption branch demonstrates a sharp rise in the amount of gas adsorbed with rising pressure, reaching a maximum adsorption point. During desorption, the amount of gas desorbed progressively declines until it reaches a particular pressure, at which point there is a sharp decrease [44]. The adsorbent could be categorized as mesoporous by IUPAC, and its average pore size was 2.32 nm. Finally, we can find that the total pore volume for La/Zn-MOF was 1.04 cc/g, average particle radius 1.52 nm, and the surfaced area  $897.69 \text{ m}^2/\text{g}$  while after adsorption of 2,4-D became pore volume 0.528 cc/g, pore radius 0.86 nm, and surface area  $560.67 \text{ m}^2/\text{g}$  respectively. The surface area and pore characteristics of the adsorbent were shown in the table, along with the fact that they decreased after 2,4-D was adsorbed. This suggests that part of the 2,4-D was eliminated through the adsorbent's pores being filled [45].

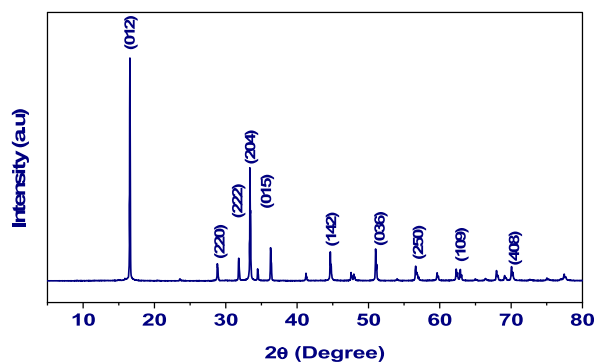


Fig. 1. XRD pattern of La/Zn-MOF.

**Table 1**  
La/Zn-MOF crystallographic data.

$2\theta_{\text{Obs.}} (^{\circ})$	$2\theta_{\text{Calc.}} (^{\circ})$	Diff.	(hkl)
16.564	16.519	0.0443	0 1 2
28.848	28.89	-0.0416	2 2 0
31.837	31.807	0.0299	2 2 2
33.418	33.395	0.0236	2 0 4
34.490	34.543	-0.0538	0 1 5
44.688	44.779	-0.0913	1 4 2
51.05	51.059	-0.0096	0 3 6
56.674	56.711	-0.0366	1 0 9
62.370	62.379	-0.0086	1 0 9
67.998	68.049	-0.0511	4 2 7
70.103	70.148	-0.0453	4 0 8

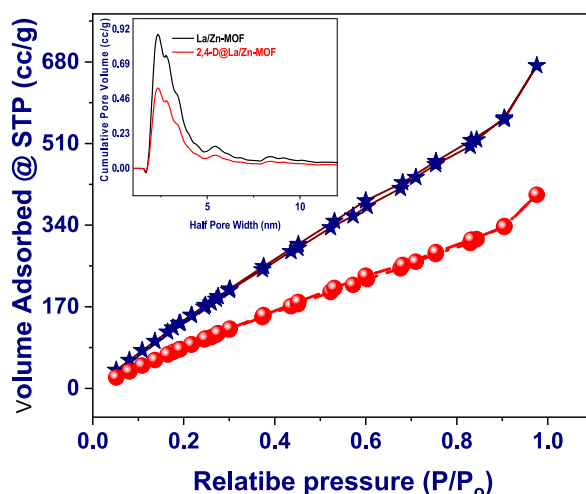


Fig. 2.  $\text{N}_2$  Adsorption/desorption isotherm of La/Zn-MOF.

### 3.1.3. FT-IR

The FT-IR spectrum of La/Zn-MOF sample prepared with La/Zn-Hmim is presented in Fig. 3. The main bands at 3425, 3132, 2908, 2767, 1615, 1582, 1415, 1365, 1089, 1029, 775, 519 and 435  $\text{cm}^{-1}$  can be demonstrated by the sample [46]. The broad band at 3425  $\text{cm}^{-1}$  might be attributed to the O-H stretching vibration of  $\text{H}_2\text{O}$  molecules that have been adsorbed on the substance's surface. The band at 3132  $\text{cm}^{-1}$  is attributed to the N-H stretching vibration of the residual Hmim [47]. Asymmetric stretching vibrations of the aromatic and aliphatic C-H were linked to the peaks located at 2908 and 2767  $\text{cm}^{-1}$ , respectively [48]. The C]C stretch mode gave rise to the band at 1615  $\text{cm}^{-1}$ , whereas the C]N stretch vibration was represented by the band at 1582  $\text{cm}^{-1}$ . The bands at 1415 and 1365  $\text{cm}^{-1}$  represented the whole ring stretching, while the aromatic C-N stretching mode was responsible for a band at 1089  $\text{cm}^{-1}$ . Likewise, the peaks located at 1029 and 775  $\text{cm}^{-1}$  may be attributed to the C-N bending vibration and the C-H bending mode,

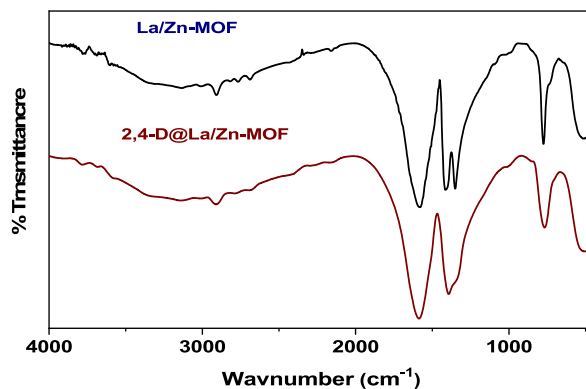


Fig. 3. FT-IR spectrum of La/Zn-MOF.

respectively. The band at  $519\text{ cm}^{-1}$  resulted from the Hmim's ring out-of-plane bending vibration. Remarkably, the La–N/Zn–N stretching vibration band at  $435\text{ cm}^{-1}$  was seen, indicating how the methylimidazole groups' nitrogen atoms combine chemically with La and Zn ions to generate imidazolate. Additionally, in the case of La/Zn-MOF, the peak at  $1843\text{ cm}^{-1}$  of the N–H stretching frequency resulting from 2-methyl imidazole is absent, indicating the bonding that exists between the ligand and metal center [49].

#### 3.1.4. SEM analysis

The SEM study that was performed to look at the morphology of the La/Zn-MOF adsorbent is shown in Fig. 4. The La/Zn-MOF adsorbent is composed of monodispersed and non-aggregated nanoparticles, as exposed by SEM pictures. Images of the material showed the presence of nanoparticles ranging in size from 50 to 150 nm. This view makes it obvious that the surface is rough and heavily ridged. There is a good possibility that the 2,4-D will be adsorbed in La–Zn MOF since it is a heterogeneous substance consisting of differently shaped nanoparticles with thick layers and pores of different sizes [50,51].

#### 3.1.5. XPS

X-ray photoelectron spectroscopy (XPS) was employed to examine the chemical conformation and binding energy characteristics of the synthesized La/Zn-MOF [52,53]. The XPS pattern of the manufactured La/Zn-MOF associated with the peaks at 284, 531, 407, 837 and 1021 eV resemble to the C1s, O1s, N1s, La3d, Zn2p and survey, respectively (Fig. 5(a–f)).

#### 3.1.6. Point of zero charge

The  $\text{pH}_{\text{PZC}}$  (point of zero charge) calculation for La/Zn-MOF resulted in a value of 7.39. This indicates that at this specific pH, the surface charge of the adsorbent becomes neutral. Once the pH exceeds this value, the surface becomes negatively charged, while at a pH lower than this value, the surface carries a positive charge (refer to Fig. S1) [40].

### 3.2. Batch research

#### 3.2.1. Consequence of pH

The 2,4-D ionization and surface features of the La/Zn-MOF are affected by the experimental pH [54]. The impact of pH was investigated across a range extending from 2 to 10, utilizing a dosage of 0.02 g of La/Zn-MOF. The experimental conditions included a 2,4-D concentration of  $1.27 \times 10^{-3}$  mmol/L, a solution volume of 25 mL, an equilibration time of 30 min, and a temperature of  $25\text{ }^{\circ}\text{C}$ , as depicted in Fig. S2. Based on the collected data, it is evident that the loading capacities of 2,4-D exhibited a significant increase as the pH level was raised from 2.0 (1.09 mmol/g) to 6.0 (1.21 mmol/g). This tendency is brought on by 2,4-D's limited solubility in acidic conditions and the fact that it exists in its difficult-to-adsorb molecular form [33,34,55]. Higher pH levels enhance the solubility and adsorption of 2,4-D as dissolved molecules because it is more hydrophilic. Up to pH 6, this impact is perceptible. But as the pH rises, the La/Zn-capacity MOFs to adsorb the dissolved 2,4-D molecules is severely harmed (Fig. S2). This consequence was qualified to the anticipated deprotonation of the practical groups in 2,4-D carboxylate, which considerably resists the charges on La/Zn-negative MOFs in these alkaline conditions [30,56]. The obtained  $\text{pH}_{\text{PZC}}$  7.39 confirms the foregoing data by showing that the La/Zn-MOF surface is saturated by negative charges overhead this pH.

#### 3.2.2. Consequence of dose

The process of 2,4-D adsorption from an aqueous solution using La/Zn-MOF was investigated through a variation in the quantities of adsorbents, ranging from 0.02 to 0.25. This adsorption study was conducted at room temperature, utilizing an original 2,4-D concentration of  $1.27 \times 10^{-3}$  mmol/L, a pH value of 6, and a contact time of 30 min. Fig. S3 illustrates how the clearance percentage of 2,4-D increased quickly as the adsorbent quantity was increased. Notably, the maximum 2,4-D elimination efficiency was observed at an adsorbent dose of 0.02 g, yielding approximately 1.227 mmol/g with a removal efficiency of 62.38%. Conversely, once the adsorbent dose was increased to 0.25 g, the adsorption capacity was 0.22 mmol/g with a removal efficiency of 96.73%. As expected, a higher dosage of adsorbents in the solution led to a greater availability of adsorption places for 2,4-D, resulting in an

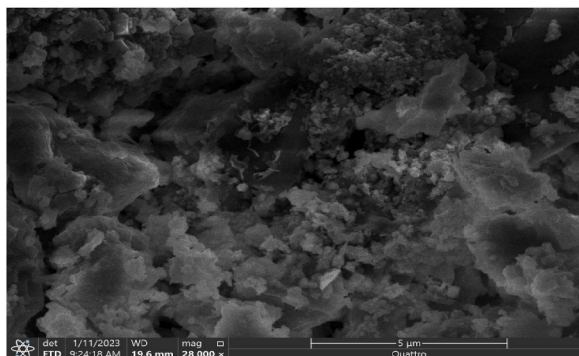


Fig. 4. SEM image of La/Zn-MOF.

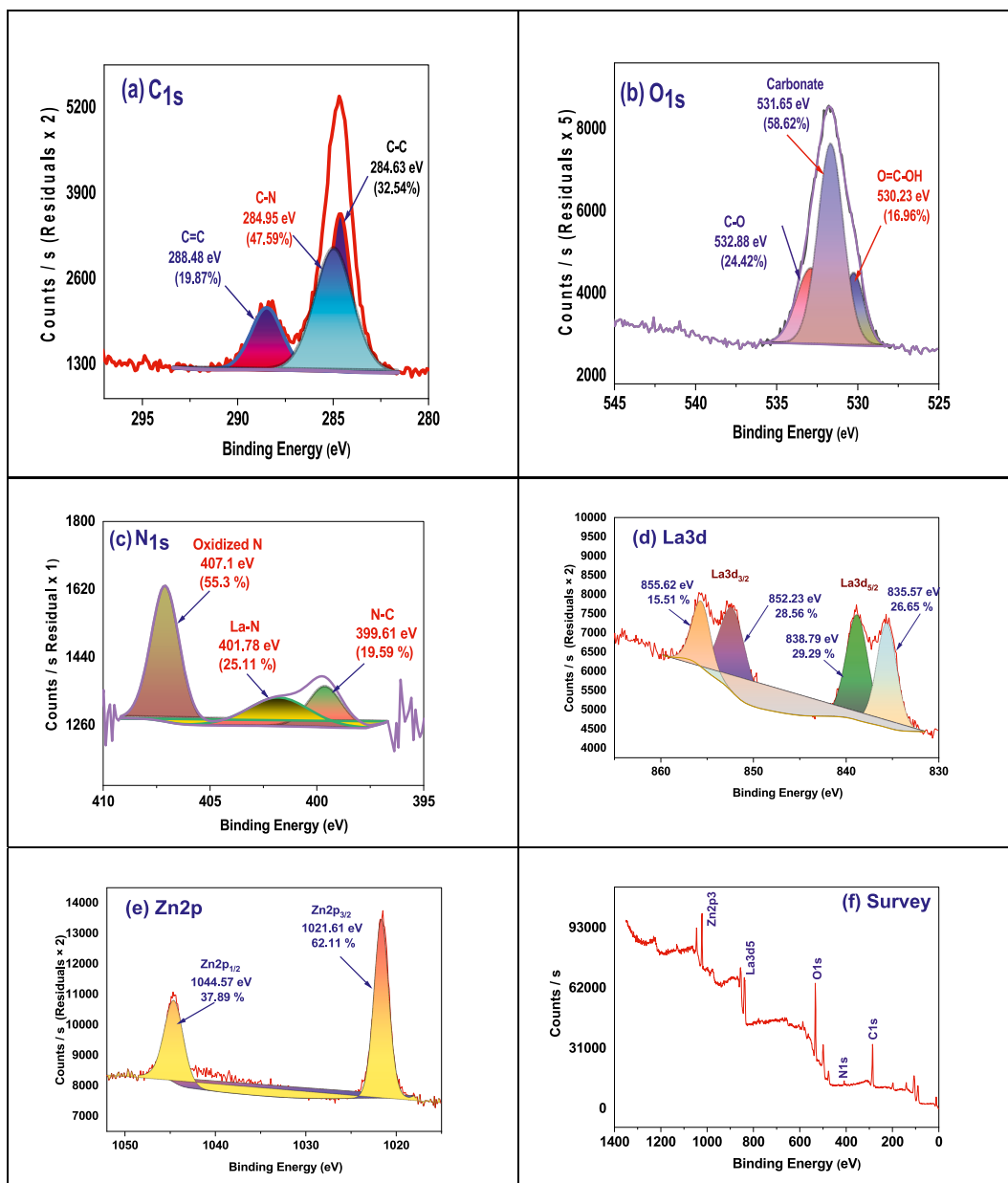


Fig. 5. XPS of La/Zn-MOF (a) C1s; (b) O1s; (c) N1s; (d) La3d; (e) Zn2p; and (f) survey.

augmented removal percentage [53]. Consequently, an adsorbent dose of 0.02 g was selected as the optimal choice for achieving higher adsorption capacity, while a dose of 0.25 g was preferred for achieving higher removal efficiency [52,53].

### 3.2.3. Consequence of 2,4-D concentration

Various 2,4-D initial concentrations, ranging from  $8.34 \times 10^{-3}$  to  $1.7 \times 10^{-3}$  mmol, were used to assess the 2,4-D elimination percentage by La/Zn-MOF (Fig. 6). The 0.02 g adsorbent was used in the adsorption research, which was approved out for 100 min at ambient temperature with a pH of 6 [30,56,57]. In general, as the original 2,4-D concentration rises, the 2,4-D clearance % falls and the equilibrium adsorption capability rises [58]. The removal efficiency and adsorption capacity both increased with concentration. A greater concentration gradient was also made possible by higher concentration levels, This is a key factor in overcoming the mass transfer impedance of the 2,4-D ion between the liquid and solid stages [40].

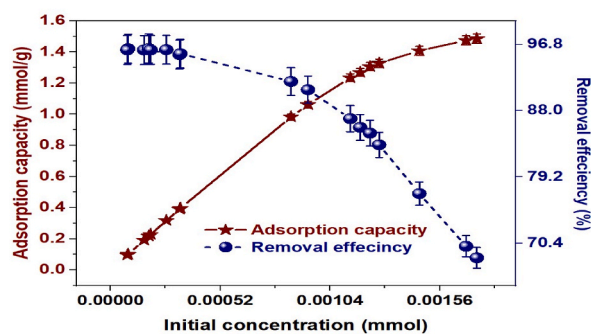


Fig. 6. Effect of the initial concentration of 2,4-D on adsorption onto La/Zn-MOF.

### 3.2.4. Consequence of contact time

The consequence of contact time on the adsorption of 2,4-D by La/Zn-MOF was investigated at pH 6, with an original concentration of 1.46 mmol/L and an adsorbent dosage of 0.02 from 0 to 100 min (Fig. S4). Due to the abundance of available adsorption sites, the quantity of 2,4-D that was adsorbed quickly increased during the early stages of the adsorption process. The saturation of the adsorption site is what causes the slowing and the creation of equilibrium [59]. At equilibrium, there are 1.53 mmol/g of 2,4-D adsorbed. For liquid phase adsorption of organic contaminants like 2,4-D, the composite La/Zn-MOF has a highly effective adsorption capacity that is caused by the large specific surface area besides pore size distribution [60].

### 3.2.5. Consequence of temperature

Temperature has a substantial impact on the adsorption process. As the temperature rises, the rate of adsorbate molecule diffusion over the intermediate pores and external boundary layer of the adsorbent molecule increases. The 2,4-D uptake varies depending on temperature, as depicted in Fig S5 below. The adsorption process may have been endothermic because the adsorption capability increases by temperature [61].

### 3.3. Adsorption isotherm

Generally, as the primary concentration was raised from  $8.3 \times 10^{-5}$  to  $1.7 \times 10^{-4}$  mmol/L, the sorption capacity of La/Zn-MOF for 2,4-D showed a progressive rise. This is explained by the fact that the porous structure of La/Zn-MOF has enough accessible unoccupied sportive sites. The decreased steric repelling forces between the adsorbed and diffused 2,4-D molecules are also responsible for this. At greater 2,4-D concentrations, there was a comparable increase in the frequency of effective collisions between 2,4-D and La/Zn-MOF (Figs. S6 and S7). As a result, due to the concentration gradient phenomena, more 2,4-D molecules were trapped within the binding sites of La/Zn-MOF. La/Zn-MOF sorbent's sorption capacity was improved as a result. With the use of the six adsorption isotherm models; Langmuir [51], Freundlich [62], Dubinin-Radushkevich [63], Temkin [64], Harkin-Jurra [65], and Redlich-Peterson [66] the experimental data was then used to evaluate the 2,4-D sorption onto La/Zn-MOF. Langmuir was fitted from the six adsorption isotherm models.

The Langmuir adsorption isotherm model is an important framework used to designate the process of molecules adhering to a solid surface. According to this model, adsorption arises on a uniform surface characterized by a finite number of identical places. The strength of attraction between the adsorbate and the surface, quantified by  $K_L$ , also referred to as the Langmuir equilibrium constant or adsorption constant (Table S4), was determined to be 136626.37 L/mmol [67]. The Freundlich model, an empirical equation, is founded on the concept of adsorption occurring on a surface with heterogeneous characteristics or containing sites with differing affinities. In this model, it's believed that the more potent binding sites are utilized first, and as the occupation of sites progresses, the binding strength tends to diminish [68]. The Freundlich constant ( $K_F$ ), which reflects the adsorbent's adsorption capacity, was calculated as  $3.45 \text{ (mmol g}^{-1}) \text{ (L.mmol}^{-1})^{1/n}$ , where  $n$  represents the Freundlich exponent [62]. This exponent acts as an indicator of the intensity of the adsorption process. The Dubinin-Radushkevich isotherm is a fundamental empirical model utilized for the description of subcritical vapor adsorption on microporous materials, particularly in scenarios where a pore-filling mechanism is at play [63]. When a particle is detached from its position within the sorption space and its binding energy, which amounts to 13.9 kJ/mol, is overcome to move it to an infinite distance, a distinction can be made between physical and chemical adsorption. In this case, the process of chemisorption is evident. The Temkin isotherm posits that, during adsorption, the most significant energy distribution of uniform bonding takes place, and as the layer becomes protected, the heat of adsorption for all particles in the phase drops linearly [64]. Where  $A_T$  is the Temkin isotherm constant was  $12.76 \text{ L mg}^{-1}$ ,  $b_T$  is the Temkin constant concerning heat of adsorption was  $8258.76 \text{ J mol}^{-1}$ .

### 3.4. Adsorption kinetics

2,4-D@La/Zn-MOF's sorption capabilities were evaluated as a function of a time range of 100 min in Figs. S8 and S9. The experimental results showed a fast increase in La/Zn-ability MOF's to adsorb 2,4-D during the first 30 min (quick initial sorption),

achieving a clearance rate of about 73.56 percent [Figs. S8 and S9](#). The concentration gradient between the vacant sportive sites/functional groups of La/Zn-MOF and the easily accessible 2,4-D molecules enabled the higher sorption rate observed during the initial phases. Additionally, the sorption rate grew gradually as the contact period increased until it reached a standstill condition (equilibrium), suggesting that no more sorption took place (reached a plateau). [Figs. S8 and S9](#) show the fitting curves and related derived parameter values for four kinetic models: pseudo-1st order [69], pseudo-2nd order [70], interarticular diffusion [71], and elovich (Table 2) [72]. The La/Zn-MOF's kinetic data in the context of sorption of 2,4-D has been effectively modeled using the pseudo-2nd order approach, revealing a strong correlation ( $R^2$  of 0.999) between experimental and model-predicted data. The application of this model suggests the presence of robust chemisorption interactions between La/Zn-MOF and 2,4-D molecules, encompassing processes like ion exchange, complexation, pore filling, and H-bonding reactions. These findings emphasize the complexity of the sorption mechanism, indicating that the La/Zn-MOF's ability to sorb 2,4-D is not merely a result of physical adsorption but involves intricate chemical reactions. The theoretical underpinning of the sorption capabilities aligns with the pseudo-2nd order model, providing insights into the underlying processes governing the interaction between La/Zn-MOF and 2,4-D.

### 3.5. Mechanism of diffusion

The sorption process typically involves three stages: intraparticle diffusion, external diffusion, and sorption reaction. Researchers used a method involving the intraparticle diffusion model to study how diazinon is adsorbed. They plotted the quantity of adsorbed diazinon ( $q_t$ ) alongside the square root of time to analyze this process ( $t^{0.5}$ ). This approach helps researchers understand how the sorption of diazinon occurs within the sorbent material. The square root of time is used because, initially, the movement of diazinon into the sorbent follows this relationship. If the plot is linear, it suggests that intraparticle diffusion is the main rate-limiting stage, but deviations from linearity could indicate other influencing factors. This method provides insights into the sorption process and its controlling mechanisms. If the plot traverses the origin, IPD is the only rate-controlling step [52,73]. Pore diffusion is not the primary factor governing the rate, though, as seen by the linear curve's failure to pass through the origin. The multilinear graph that was seen during the sorption procedure suggests that 2,4-D may have been deposited onto the La/Zn-MOF sorbent through both film diffusion and surface sorption. The width of the boundary layer, which increased as the 2,4-D content increased, had an impact on the mass transfer rate to the outside surface. According to the information [Table 2](#), the beginning concentration for the kinetic investigation was  $1.46 \times 10^{-3}$  mmol/L, the temperature was 25 °C, and the contact period lasted 90 min ([Fig. 7](#)).

### 3.6. Adsorption thermodynamics

The result of temperature on 2,4-D@La/Zn-MOF's adsorption from aqueous solutions is shown in [Fig. S10](#). The adsorption capacity increases at higher temperatures because the molecules are more mobile at that temperature. The environment's accelerating molecules improved the kinetic energy of the speedy molecules, which now had kinetic energy. When the molecules come across mesopores with additional surface area, they can switch to the holes quickly. At the six temperatures, the concentration of 2,4-D with the

**Table 2**  
The 2,4-D adsorption onto La/Zn-MOF, adsorption kinetic parameter.

Model	Parameter values		
	Linear		Non-Linear
Pseudo-First-order kinetic	$K_1$ ( $\text{min}^{-1}$ )	0.009	0.005
	$q_e$ ( $\text{mmol.g}^{-1}$ )	0.6	0.82
	Reduced Chi-Sqr	17.76	72.67
	Residual Sum of Squares	302.05	1284.8
	Root-MSE (SD)	4.22	6.66
	$R^2$	0.945	0.93
Pseudo-second-order kinetic	$K_2$ ( $\text{g mg}^{-1}\text{min}^{-1}$ )	0.075	0.1
	$q_e$ ( $\text{mmol.g}^{-1}$ )	1.54	1.54
	Reduced Chi-Sqr	2.367	8.56
	Residual Sum of Squares	42.62	158.27
	Root-MSE (SD)	1.538	2.98
	$R^2$	0.993	0.996
Intraparticle diffusion	$K_i$ ( $\text{mgg}^{-1}\text{min}^{1/2}$ )	0.065	0.04
	$X$ ( $\text{mg.g}^{-1}$ )	0.87	0.62
	Reduced Chi-Sqr	7.88	18.21
	Residual Sum of Squares	139.486	328.43
	Root-MSE (SD)	2.78	3.82
	$R^2$	0.878	0.724
Elovich	$\beta$ ( $\text{g/mg}$ )	6.45	3.88
	$\alpha$ ( $\text{mgg}^{-1}\text{min}^{-1}$ )	2.09	1.84
	Reduced Chi-Sqr	1.29	16.83
	Residual Sum of Squares	26.79	312.6
	Root-MSE (SD)	1.36	3.18
	$R^2$	0.92	0.98
Test results	$q_e$ (exp) ( $\text{mmol.g}^{-1}$ )	1.53	1.53

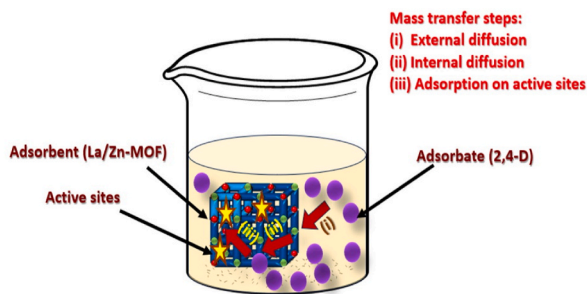


Fig. 7. Diffusion mechanism of 2,4-D onto La/Zn-MOF.

best elimination percentage was 1.46 mmol/L, and the removal values rose with temperature. The optimum removal values were found at the maximum temperature of 318 K. Table 3 lists the thermodynamic characteristics for 2,4-D adsorption on La/Zn-MOF, with the Gibbs free energy ( $\Delta G^\circ$ ), entropy ( $\Delta S^\circ$ ) and enthalpy ( $\Delta H^\circ$ ) standards. The intercept and slope of the plot of  $\ln K_c$  and versus  $1/T$ , respectively, were used to estimate the values of  $\Delta S^\circ$  and  $\Delta H^\circ$  (Fig. S10). Standards of  $\Delta G^\circ$  ranged from  $-0.49$  to  $-5.5$  kJ/mol. The spontaneous character of 2,4-D adsorption onto La/Zn-MOF and the feasibility of this removal technique are both demonstrated by the negative  $\Delta G^\circ$  values.  $\Delta G^\circ$  values were calculated as well for each of the three temperatures; these values increased with temperature, indicating that this separation mechanism is most effective at high temperatures. Accordingly, electrostatic interactions, chemical bonds, and van der Waals forces between 2,4-D and La/Zn-MOF are the causes of the rise in 2,4-D removal with rising temperature. 2,4-D elimination with La/Zn-MOF resulted in  $\Delta H^\circ$  values of  $58.28$  kJ mol $^{-1}$  and  $\Delta S^\circ$  values of  $200.62$  J mol $^{-1}$ K $^{-1}$  being estimated. Positive  $\Delta H^\circ$  and  $\Delta S^\circ$  values establish greater randomness at the adsorbent-2,4-D interface and La/Zn-MOF affinity for 2,4-D, demonstrating the endothermic nature of the removal procedure [74].

### 3.7. Mechanism of interaction

A clearer knowledge of the most likely verified mechanisms behind the sorption of 2,4-D onto La/Zn-MOF was achieved by combining physicochemical analysis, sorption data, and theoretical models. This naturally generated adsorbent is well known for having a significant capacity for the exchange of ions, particularly with 2,4-D pollutants. The increased sorption of 2,4-D molecules may be attributed to the electrostatic interactions among the several functional groups of La/Zn MOF, that competed with the functional groups of 2,4-D molecules (attraction and amide group). The heterogeneous characteristic deduced from the La/Zn MOF kinetic modeling is explained by this finding. By exchanging ( $-\text{OH}^-$ ) groups on the surface, La/Zn-MOF and 2,4-D molecules were able to create mononuclear monodentate and binuclear bidentate inner-sphere complexes, which proved to be more effective than other sorbents, according to the results of the experimental sorption. The SEM results also revealed a smoother and more compact La/Zn-MOF surface after 2,4-D sorption, which can be related to pore blockage. Furthermore, the BET analysis verified that the adsorbent's pore size as well as surface area had shrunk [75]. This phenomenon indicates that the sorption of 2,4-D involved both surface complexation as well as the pore-filling action mechanism (Fig. 8).

### 3.8. Consequence of salinity

Understanding and improving pollutant adsorption depends on understanding ionic strength because it discloses electrostatic interactions, solution chemistry, and treatment effectiveness in intricate environmental matrices. To accurately represent the elements present in industrial wastewater, Fig. S11 assessment of the sorption efficiency (percent) index of the La/Zn-MOF sorbent towards 2,4-D molecules in the attendance of dissolved background ions (NaCl) is sufficient. In the multi-component system Fig. S11, there was a small decrease in the 2,4-D removal (from 99.5 to 88.2 percent) by La/Zn-MOF sorbent. This can be accredited to the impact of NaCl, which shields surface-active places by altering the 2,4-D solubility and raising the ionic strength of the aqueous media [76].

Table 3  
Thermodynamic limits of adsorption 2,4-D on La/Zn-MOF.

Adsorbate	T (K)	$\Delta H^\circ$ (kJ.mol $^{-1}$ )	$\Delta S^\circ$ (J.mol $^{-1}$ K $^{-1}$ )	$-\Delta G^\circ$ (kJ.mol $^{-1}$ )
2,4-D	298	58.28	200.2	0.49
	303			1.49
	308			2.49
	313			4.5
	318			5.5

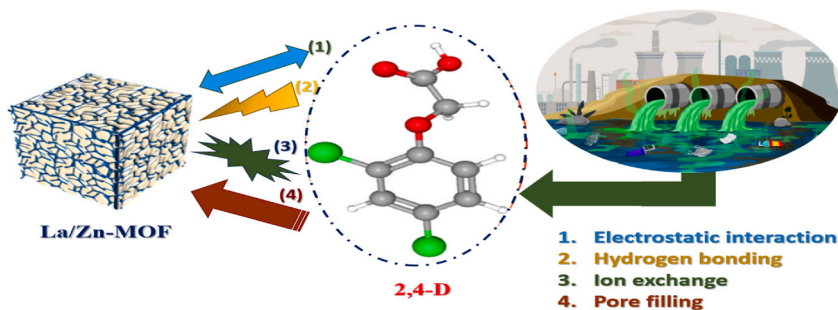


Fig. 8. Interaction mechanism between La/Zn-MOF and 2,4-D.

### 3.9. Recyclability and environmental application

Assessing recyclability plays an energetic role in gauging the potential applications of adsorbents. As depicted in Fig. S12, the regenerated La/Zn-MOF exhibited efficient adsorption performance for 2,4-D, with the removal rate maintaining stability even after undergoing 5 cycles. As a result of its exceptional stability and reusability during the adsorption process, La/Zn-MOF is demonstrated to be a suitable adsorbent for the removal of 2,4-D. The reusability of adsorbents is essential for industrial applications since desorption is a major factor in adsorbent regeneration. The effectiveness of desorption was improved by examining how the pH of the desorption solvent affected the elimination of adsorbed 2,4-D from La/Zn-MOF. To evaluate the La/Zn-practical MOF's use in real samples, 2,4-D was injected into lake water and control water in a range of dosages. In Fig. S12, the removal rates are displayed. According to the findings, the clearance rates for the control water, which ranged from 88.35 percent to 98.56 percent, and the spiked lake water, which ranged from 87.4 percent to 98.2 percent, were both satisfactory. La/Zn-MOF showed a similar 2,4-D elimination rate, which indicates that 2,4-D adsorption from lake water is conceivable. Additionally, 2,4-D was completely removed from both lake and control water at values below 40 mg/L, illustrating the greater adsorption capacity of La/Zn-MOF. But when the original concentrations were 40 mg/L and 80 mg/L, respectively, 2,4-D was eliminated by around 98.5 percent and 82 percent. The removal rate decreased as 2,4-D concentrations increased because there were fewer active sites on the adsorbent surface to handle higher doses of 2,4-D [77].

### 3.10. Relative to alternative adsorbents

Table S5 compares the maximum sorption capacities of the La/Zn-MOF sorbent with different values obtained from the available research, along with the associated reported ideal operating parameters. While the differences in experimental settings make direct comparisons of sorption performance difficult, this criterion is nonetheless appropriate for a broad evaluation of these materials' potential. The La/Zn-MOF sorbent is particularly advantageous because of its quick kinetics. It is important to note that the La/Zn-MOF shows a considerable capability to bind with 2,4-D, suggesting that it might be used for the treatment of wastewater, especially for the removal of this chemical from water sources [77].

### 3.11. Statistical evaluation

Table S6 demonstrates the findings of the RSM investigation that was performed. Using the experimental adsorption capacity, the coefficients of the response surface equation were determined. The least squares method was used to determine the reversion coefficients for the intercept, quadratic, linear, and interaction terms of the model, which are revealed in Table S6.  $R^2 = 0.994$  indicates that the obtained second-order polynomial equation (Eqs. (3) and (4)) adequately represents the investigational data. The analysis of variability for the results of the BBD study is also shown in Table S7. The standards of  $\text{adj-}R^2$  and predictable  $R^2$  were 0.9067 and 0.9901, individually (Table S8). A high  $R^2$  value suggests that the variance might be satisfactorily explained by the information appropriate to the model. Smaller 2,4-D readings provide improved reproducibility since they express the standard unconventionality as a quantity of the mean. The model was repeatable, as evidenced by the coefficient of dissimilarity (2,4-D), which was less than 10. Predicted Residual Sum of Squares (PRESS), a measurement of how well a specific model fits each fact in the design, was 0.0466 for the model. The model's inferred significance was indicated by its model F-value of 246.16 [78].

The significance of the model becomes evident through its substantial Model F-value of 246.16. Such a large F-value suggests that this occurrence due to random variation is plausible only in 0.01 percent of belongings. Model relations are deemed noteworthy if their corresponding P-value is less than 0.0500. In this particular situation, the terms A, B, C, and  $A^2$  are all noteworthy model terms. Conversely, model relations are considered irrelevant when their value exceeds 0.1000. If your model contains numerous unnecessary terms (excluding those necessary for maintaining hierarchy), reducing the model may be beneficial. The importance of the lack of fit is underscored by the sizable Lack of Fit F-value of 246.16. A high Lack of Fit F-value signifies a mere 0.01 percent probability of noise, highlighting its exceptionally low likelihood.

The disparity among the Predicted  $R^2$ , which stands at 0.9067, and the familiar  $R^2$ , which is recorded at 0.9901, falls within the range of less than 0.2. This level of agreement is generally considered reasonable. Adequate Precision (Adeq Precision) serves as a gauge of the signal-to-noise ratio. A ratio of 4 or higher is typically favored. In your case, the signal strength is substantial, as evidenced

by your ratio of 63.557. To navigate the design space using this approach, Table S9 can be a valuable resource [28].

The formula with codes:

$$q_c = 1.267 + -0.033975xA + 0.23165xB + -0.036825xC + -0.00645xAB + 0.0029xAC + -0.01325xBC + -0.0727xA^2 + -0.04935xB^2 + 0.0136 \times C^2 \tag{3}$$

The actual formula:

$$q_c = 0.87726 + 0.0469624xpH + 0.00770461xtime + -0.508354xDose + -0.0000339474xpHxtime + 0.00630435xpHxDose + -0.00242563xtimexDose + -0.00454375xpH^2 + -0.0000218726xtime^2 + 1.02836 \times Dose^2 \tag{4}$$

According to Fig. S13, the anticipated values derived from Eqs. (3) and (4) were in brilliant agreement with the experimental consequences. Thus, the tested design fits well with this quadratic model.

### 3.12. Optimization of adsorption of 2,4-D on La/Zn MOF

The best way to convey the impact of any parameter on the adsorption capacity inside the experimental space under investigation was to create response surface graphs of the equation. Plotting response surfaces allowed researchers to investigate the impact of different parameters and their interactions on the adsorption capacity using Design-Expert software (version 9.0.4.1). In Fig. 9(a–c),

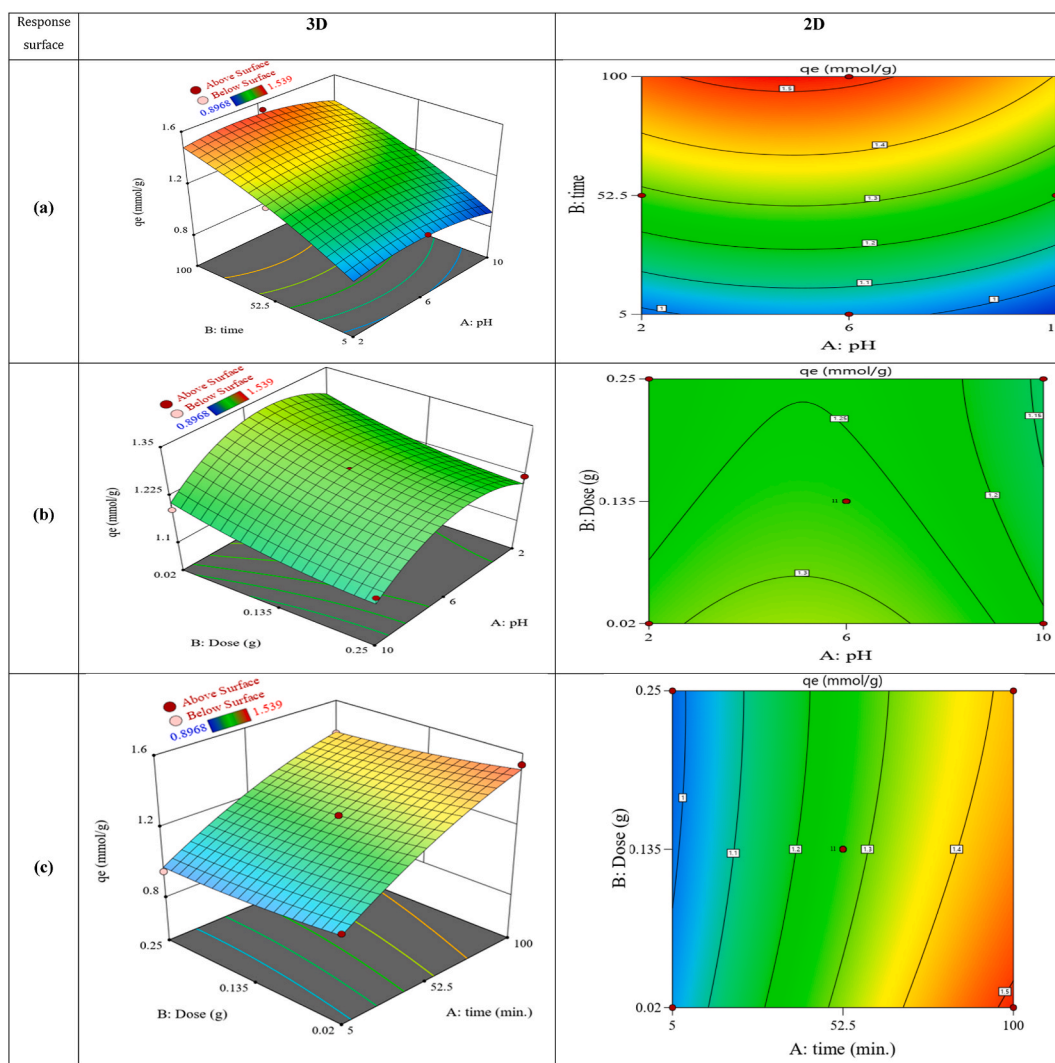


Fig. 9. Both 2D and 3D response surface (a–c).

the effects of time, pH, and temperature on adsorption capability are shown [31].

In Fig. 9(a), both the 3D response surface design and the contour plot were constructed to illustrate the relationship between adsorption capacity and changes in the time and pH. It became evident that the adsorption capability exhibited a clear increase with longer durations of time and a decrease in pH values. Notably, the optimal adsorption situations were detected in an acidic environment with a pH of 6 and a period of 100 min. The adsorption capability was 1.53 mmol/g under these circumstances. In Fig. 9(b), to demonstrate the link between capacities for adsorption, changing time, and various dosages ranging from 0.02 to 0.25 g, two 3D response surface plots and a contour plot were made. It is apparent from the plots that an increase in the dose leads to a reduction in adsorption capability, accompanied by an increase in removal efficiency. In Fig. 9(c), the influence of both time and dose on adsorption capacity is depicted. It's evident that as the duration of time increases, there is a corresponding increase in adsorption capacity.

In conclusion, the optimal adsorption conditions for 2,4-D onto La/Zn MOF were determined to be at pH 6, a time of 100 min, and a dose of 0.02 g. Under these optimized circumstances, the predicted adsorption capability was found to be 1.53 mmol/g [56].

### 3.13. Perturbation plot

Every variable is compared at a selected point in the well-considered design space using the perturbation plot. Fig. 10(a) exhibits the perturbation design for the 2,4-D adsorption capacity onto La/Zn-MOF. The yield response was determined by varying only one element over its range while keeping the other parameters constant. The plot illustrates the relative contributions of time, dosage, and pH to each component at a critical point in the design space (Fig. 10(b)). Each variable appears to have a positive effect on the adsorption capacity. The enormous curvature influence that time, pH, and dosage had is shown by the perturbation figure in Table S10 and Eqs. (3) and (4). The adsorption capacity adjusted to all of these variables quite quickly, as evidenced by the link between pH and the adsorption procedure's time. To determine which parameter was most crucial, the coefficients in Eq. (4) were associated. The observed adsorption capacity response was positively influenced by the adsorption process's time, pH, and dosage in this order of increasing strength [30].

### 3.14. Model adequacy checking

To make sure the fitted model accurately approximates the real system, it is typically necessary to check it. If the model does not show a suitable fit, the analysis and optimization of the fitted response surface will likely be carried out with inadequate or erroneous results. When assessing a model's appropriateness, residuals that result from the smallest squares fit are extremely important. Using the residuals to create a normal probability diagram, the presumption of normality was examined (Fig. 10(c)). The hypothesis of normality was supported by the residual chart, which essentially showed a straight line. Fig. 10(d) provides a visual representation of the residuals compared to the expected reaction. It appears that the residuals are randomly distributed throughout the display, suggesting that the variation of the first observation is constant for every value of  $q_e$ . Given the good plots (Fig. 10(c and d)), we conclude that the empirical model adequately describes the adsorption procedure via the response surface [34].

### 3.15. Validation of the model

To contrast the expected outcome with the real result, the rechecking test was carried out using one or more extraction circumstances. As a result of actual experiments, the results showed that the RSM model was exact because there were no significant variations ( $p > 0.05$ ) (Table S10). The response model was adequate to reflect the anticipated adsorption capability condition, as evidenced by the good relationship between the actual and expected definitions [35,38].

## 4. Conclusion

The purpose of this effort was to examine the equilibrium behavior of adsorption of 2,4-dichlorophenylacetic acid (2,4-D) onto hetero bimetallic organic frameworks (MOFs) based on zinc and lanthanum (called La/Zn-MOF). The results of the study displayed that there was a significant decrease in the surface area of La/Zn-MOF after 2,4-D was adsorbed. Despite the substance's initial properties, which included a significant surface area and pore volume before the adsorption development, this was noted. The reduction in surface area and pore volume makes it clear that the adsorption occurred inside the adsorbent's pores. The La/Zn-MOF exhibited a relatively large surface area (897.69 m<sup>2</sup>/g) and pore volume (1.04 cm<sup>3</sup>/g) and succeeding the adsorption of 2,4-D, the surface area and pore volume of La/Zn-MOF decreased to 560.67 m<sup>2</sup>/g and 0.58 cm<sup>3</sup>/g, respectively. The kinetic analysis showed that when compared to other kinetic models, the second-order model produced enhanced results. Furthermore, the diffusional model offered a precise forecast of the concentration variations throughout time. The Langmuir adsorption isotherm model fitting the adsorption isotherm study, and the thermodynamic properties demonstrated that the adsorption process was spontaneous and endothermic. Analyzing the variations in pH of the solution throughout the 2,4-D adsorption process onto La/Zn-MOF exposed a noteworthy relationship between pH values and the amount of adsorption. Notably, a pH of 6 was shown to be perfect for adsorption. The greatest adsorption capacity ever recorded was 307.5 mg/g in circumstances close to a pH of 6. The Box-Behnken design was used to optimize the adsorption performance.

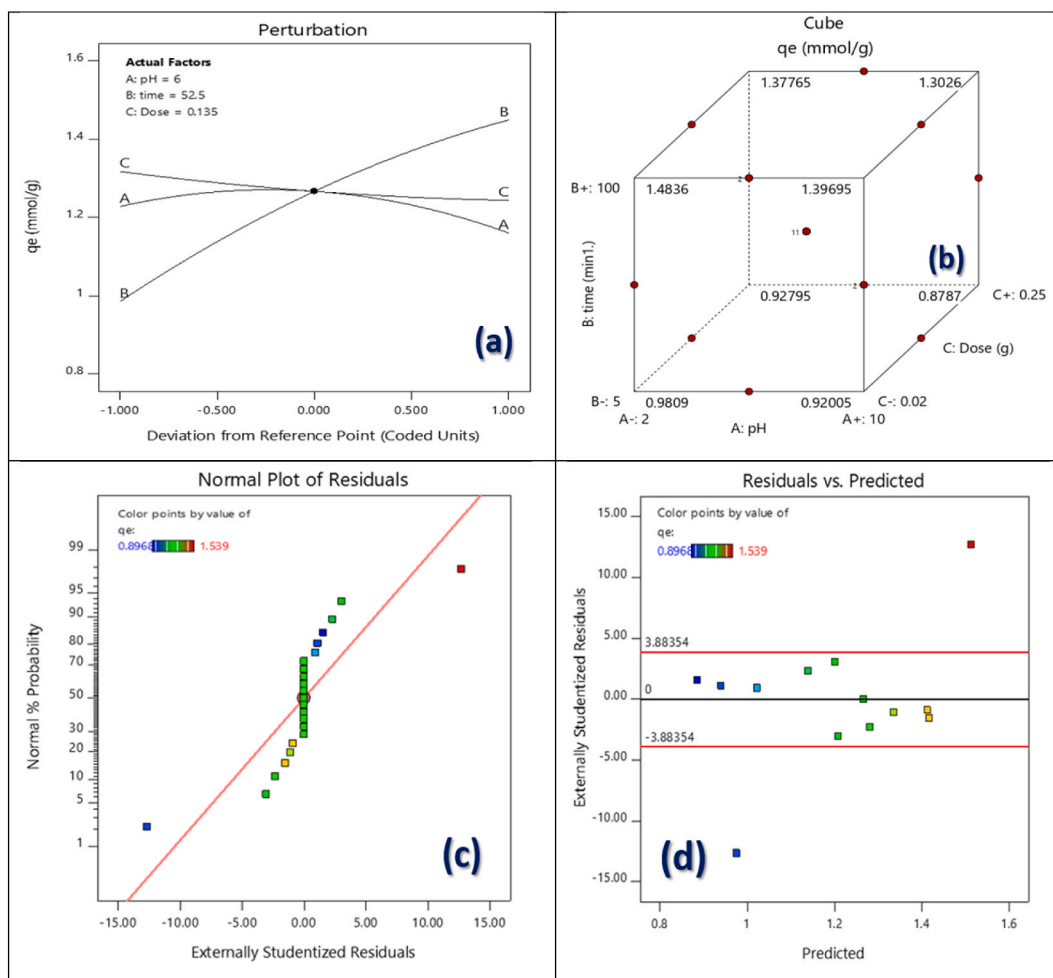


**Fig. 10.** (a) Plot for perturbation in rate of response (for A: pH, B: time and C: Dose), (b) Cubic graphical optimization of adsorption capacity, (c) Normal plot of residual, (d) Residuals vs. Predicted.

### Data availability

Data will be made available on request.

### CRediT authorship contribution statement

**Omaymah Alaysuy:** Writing – original draft, Validation, Investigation, Data curation. **Meshari M. Aljohani:** Validation, Resources, Methodology, Investigation. **Kholood Alkhamis:** Writing – original draft, Software, Methodology, Funding acquisition. **Nada M. Alatawi:** Visualization, Validation, Software, Resources. **Awatif R.Z. Almotairy:** Visualization, Software, Resources, Methodology. **Kholood A. Abu Al-Ola:** Visualization, Resources, Methodology. **Abdelrahman S. Khder:** Writing – original draft, Visualization, Software, Resources. **Nashwa M. El-Metwaly:** Writing – review & editing, Supervision, Project administration, Funding acquisition.

### Declaration of competing interest

The authors declare that they have no known competing financial interests or personal relationships that could have appeared to influence the work reported in this paper.

### Appendix A. Supplementary data

Supplementary data to this article can be found online at <https://doi.org/10.1016/j.heliyon.2024.e28622>.

## References

- [1] M.A. Rippy, A. Deletic, J. Black, R. Aryal, J.-L. Lampard, J.Y.-M. Tang, D. McCarthy, P. Kolotelo, J. Sidhu, W. Gernjak, Pesticide occurrence and spatio-temporal variability in urban run-off across Australia, *Water Res.* 115 (2017) 245–255, <https://doi.org/10.1016/j.watres.2017.03.010>.
- [2] J. Cai, M. Zhou, X. Du, X. Xu, Enhanced mechanism of 2, 4-dichlorophenoxyacetic acid degradation by electrochemical activation of persulfate on Blue-TiO<sub>2</sub> nanotubes anode, *Separ. Purif. Technol.* 254 (2021) 117560, <http://doi:10.1016/j.seppur.2020.117560>.
- [3] A. Azari, M. Abtahi, S. Dobaradaran, R. Saeedi, A.R. Yari, M.H. Vaziri, S.A. Razavinasab, M. Malakoutian, K. Yaghmaein, N. Jaafarzadeh, Polycyclic aromatic hydrocarbons in high-consumption soft drinks and non-alcoholic beers in Iran: monitoring, Monte Carlo simulations and human health risk assessment, *Microchem. J.* 191 (2023) 108791, <http://doi:10.1016/j.microc.2023.108791>.
- [4] J.P. Fry, D.C. Love, G.K. MacDonald, P.C. West, P.M. Engstrom, K.E. Nachman, R.S. Lawrence, Environmental health impacts of feeding crops to farmed fish, *Environ. Int.* 91 (2016) 201–214, <https://doi.org/10.1016/j.envint.2016.02.022>.
- [5] M.A. Zazouli, A. Azari, S. Dehghan, R. Salmani Malekkolae, Adsorption of methylene blue from aqueous solution onto activated carbons developed from eucalyptus bark and Crataegus oxyacantha core, *Water Sci. Technol.* 74 (2016) 2021–2035, <https://doi.org/10.1016/j.watres.2016.02.017>.
- [6] G.B.F. Salla, L. Bracht, A.V. Parizotto, J.F. Comar, R.M. Peralta, F. Bracht, A. Bracht, Kinetics of the metabolic effects, distribution spaces and lipid-bilayer affinities of the organo-chlorinated herbicides 2, 4-D and picloram in the liver, *Toxicol. Lett.* 313 (2019) 137–149, <https://doi.org/10.1016/j.toxlet.2019.06.008>.
- [7] J.-C. Sin, S.-M. Lam, H. Zeng, H. Lin, H. Li, A.K. Kumaresan, A.R. Mohamed, J.-W. Lim, Z-scheme heterojunction nanocomposite fabricated by decorating magnetic MnFe<sub>2</sub>O<sub>4</sub> nanoparticles on BiOBr nanosheets for enhanced visible light photocatalytic degradation of 2, 4-dichlorophenoxyacetic acid and Rhodamine B, *Separ. Purif. Technol.* 250 (2020) 117186, <https://doi.org/10.1016/j.seppur.2020.117186>.
- [8] W. Abd El-Fattah, A. Guesmi, N.B. Hamadi, M.G. El-Desouky, A. Shahat, A green synthesis of cellulose nanocrystals biosorbent for remediation of wastewater containing industrial dye, *Colloids Surf. A Physicochem. Eng. Asp.* 681 (2024) 132729, <https://doi.org/10.1016/j.colsurfa.2023.132729>.
- [9] A.E. Gonzalez, M. Asomoza, S. Solís, M.A.G. Sánchez, S. Cipagauta-Diaz, Enhanced photocatalytic degradation of the herbicide 2, 4-dichlorophenoxyacetic acid by Pt/TiO<sub>2</sub>-SiO<sub>2</sub> nanocomposites, *React. Kinet. Mech. Catal.* 131 (2020) 489–503, <https://doi.org/10.1007/s11144-020-01865-x>.
- [10] F.H. Tang, M. Lenzen, A. McBratney, F. Maggi, Risk of pesticide pollution at the global scale, *Nat. Geosci.* 14 (2021) 206–210, <https://doi.org/10.1038/s41561-021-00712-5>.
- [11] D. Samir, C. Khemissi, Application of geothermometric and hydrochemical methods to the investigation of thermal water of sources in the Northeastern of Algeria case of Setif city, *Journal of Umm Al-Qura University for Applied Sciences* 8 (2022) 2731–6734, <http://doi:10.1007/s43994-022-00005-6>.
- [12] D. Han, W. Jia, H. Liang, Selective removal of 2, 4-dichlorophenoxyacetic acid from water by molecularly-imprinted amino-functionalized silica gel sorbent, *J. Environ. Sci.* 22 (2010) 237–241, [https://doi.org/10.1016/S1001-0742\(09\)60099-1](https://doi.org/10.1016/S1001-0742(09)60099-1).
- [13] R. Vinayagam, S. Pai, G. Murugesan, T. Varadavenkatesan, S. Narayanasamy, R. Selvaraj, Magnetic activated charcoal/Fe<sub>2</sub>O<sub>3</sub> nanocomposite for the adsorptive removal of 2, 4-Dichlorophenoxyacetic acid (2, 4-D) from aqueous solutions: synthesis, characterization, optimization, kinetic and isotherm studies, *Chemosphere* 286 (2022) 131938, <https://doi.org/10.1016/j.chemosphere.2021.131938>.
- [14] H.M. Nassef, G.A. Al-Hazmi, A.A. Alayyafi, M.G. El-Desouky, A.A. El-Bindary, Synthesis and characterization of new composite sponge combining of metal-organic framework and chitosan for the elimination of Pb (II), Cu (II) and Cd (II) ions from aqueous solutions: batch adsorption and optimization using Box-Behnken design, *J. Mol. Liq.* 394 (2024) 123741, <https://doi.org/10.1016/j.molliq.2023.123741>.
- [15] M.L. Hladik, A.L. Roberts, E.J. Bouwer, Removal of neutral chloroacetamide herbicide degradates during simulated unit processes for drinking water treatment, *Water Res.* 39 (2005) 5033–5044, <https://doi.org/10.1016/j.watres.2005.10.008>.
- [16] X. Yang, T. Muhammad, J. Yang, A. Yasen, L. Chen, In-situ kinetic and thermodynamic study of 2, 4-dichlorophenoxyacetic acid adsorption on molecularly imprinted polymer based solid-phase microextraction coatings, *Sensor Actuator Phys.* 313 (2020) 112190, <https://doi.org/10.1016/j.sna.2020.112190>.
- [17] V.S. Priya, S.K. Basha, V.S. Kumari, Kinetics and adsorption performance of biosorbent starch/poly (vinyl alcohol)/graphene oxide nanocomposite for the removal of dyes, *Journal of Umm Al-Qura University for Applied Sciences* 9 (2023) 529–547, <https://doi.org/10.1007/s43994-023-00063-4>. %@ 2731-6734.
- [18] N. Hassan, A.Z. El-Sonbati, M.G. El-Desouky, Synthesis, characterization, molecular docking and DNA binding studies of Cu(II), Ni(II), Zn(II) and Mn(II) complexes, *J. Mol. Liq.* 242 (2017) 293–307, <https://doi.org/10.1016/j.molliq.2017.07.019>.
- [19] H. Wang, J. Wang, J. Wang, R. Zhu, Y. Shen, Q. Xu, X. Hu, Spectroscopic method for the detection of 2, 4-dichlorophenoxyacetic acid based on its inhibitory effect towards catalase immobilized on reusable magnetic Fe<sub>3</sub>O<sub>4</sub>-chitosan nanocomposite, *Sensor. Actuator. B Chem.* 247 (2017) 146–154, <https://doi.org/10.1016/j.snb.2017.02.175>.
- [20] S. Abd El Wanees, M.M. Kamel, M. Ibrahim, S.M. Rashwan, Y. Atef, M.G. Abd Elsadek, Corrosion Inhibition and Synergistic Effect of Ionic Liquids and Iodide Ions on the Corrosion of C-Steel in Formation Water Associated with Crude Oil, *Journal of Umm Al-Qura University for Applied Sciences*, 2023, pp. 1–13, <https://doi.org/10.1007/s43994-023-00084-z>. %@ 2731-6734.
- [21] O. Kazak, Y.R. Eker, I. Akin, H. Bingol, A. Tor, Green preparation of a novel red mud@ carbon composite and its application for adsorption of 2, 4-dichlorophenoxyacetic acid from aqueous solution, *Environ. Sci. Pollut. Control Ser.* 24 (2017) 23057–23068, <https://doi.org/10.1007/s11356-017-9937-x>.
- [22] H. Wang, Q. Xu, J. Wang, W. Du, F. Liu, X. Hu, Dendrimer-like amino-functionalized hierarchical porous silica nanoparticle: a host material for 2, 4-dichlorophenoxyacetic acid imprinting and sensing, *Biosens. Bioelectron.* 100 (2018) 105–114, <https://doi.org/10.1016/j.bios.2017.08.063>.
- [23] X. Wang, J. Yu, X. Wu, J. Fu, Q. Kang, D. Shen, J. Li, L. Chen, A molecular imprinting-based turn-on ratiometric fluorescence sensor for highly selective and sensitive detection of 2, 4-dichlorophenoxyacetic acid (2, 4-D), *Biosens. Bioelectron.* 81 (2016) 438–444, <https://doi.org/10.1016/j.bios.2016.03.031>.
- [24] H. Luo, X. Zhou, Q. Chen, J. Zhou, Removal of 2, 4-dichlorophenoxyacetic acid by the boron-nitrogen co-doped carbon nanotubes: insights into peroxymonosulfate adsorption and activation, *Separ. Purif. Technol.* 259 (2021) 118196, <https://doi.org/10.1016/j.seppur.2020.118196>.
- [25] J. Zuo, B. Wang, J. Kang, P. Yan, J. Shen, S. Wang, D. Fu, X. Zhu, T. She, S. Zhao, Activation of peroxymonosulfate by nanoscaled NiFe<sub>2</sub>O<sub>4</sub> magnetic particles for the degradation of 2, 4-dichlorophenoxyacetic acid in water: efficiency, mechanism and degradation pathways, *Separ. Purif. Technol.* 297 (2022) 121459, <https://doi.org/10.1016/j.seppur.2022.121459>.
- [26] C. Lin, Y. Qiu, J. Fan, M. Wang, L. Ye, Y. Liu, X. Ye, X. Huang, Y. Lv, M. Liu, Fabrication of photo-responsive cellulose based intelligent imprinted material and selective adsorption on typical pesticide residue, *Chem. Eng. J.* 394 (2020) 124841, <https://doi.org/10.1016/j.cej.2020.124841>.
- [27] G.A.A. AlHazmi, K.S. AbouMelha, M.G. El-Desouky, A.A. El-Bindary, Effective adsorption of doxorubicin hydrochloride on zirconium metal-organic framework: equilibrium, kinetic and thermodynamic studies, *J. Mol. Struct.* (2022) 1258, <https://doi.org/10.1016/j.molstruc.2022.132679>.
- [28] A. Almahri, M. Morad, M.M. Aljohani, N.M. Alatawi, F.A. Saad, H.M. Abumelha, M.G. El-Desouky, A.A. El-Bindary, Atrazine reclamation from an aqueous environment using a ruthenium-based metal-organic framework, *Process Saf. Environ. Protect.* 177 (2023) 52–68, <https://doi.org/10.1016/j.psep.2023.06.091>.
- [29] G.A. Al-Hazmi, A.A. Alayyafi, M.G. El-Desouky, A.A. El-Bindary, Guava seed activated carbon loaded calcium alginate aerogel for the adsorption of diclofenac sodium: characterization, isotherm, kinetics, and optimization via Box-Behnken design, *Int. J. Biol. Macromol.* (2024) 129995, <https://doi.org/10.1016/j.ijbiomac.2024.129995>.
- [30] S.H. Alrefaee, M. Aljohani, K. Alkhamis, F. Shaaban, M.G. El-Desouky, A.A. El-Bindary, M.A. El-Bindary, Adsorption and effective removal of organophosphorus pesticides from aqueous solution via novel metal-organic framework: adsorption isotherms, kinetics, and optimization via Box-Behnken design, *J. Mol. Liq.* 384 (2023), <https://doi.org/10.1016/j.molliq.2023.122206>.
- [31] M.M. Aljohani, S.D. Al-Qahtani, M. Alshareef, M.G. El-Desouky, A.A. El-Bindary, N.M. El-Metwaly, M.A. El-Bindary, Highly efficient adsorption and removal bio-staining dye from industrial wastewater onto mesoporous Ag-MOFs, *Process Saf. Environ. Protect.* 172 (2023) 395–407, <https://doi.org/10.1016/j.psep.2023.02.036>.
- [32] A.M. Alsuhaibani, A.A. Alayyafi, L.A. Albedair, M.G. El-Desouky, A.A. El-Bindary, Synthesis and characterization of metal-organic frameworks based on thorium for the effective removal of 2, 4-dichlorophenylacetic pesticide from water: batch adsorption and Box-Behnken Design optimization, and evaluation of reusability, *J. Mol. Liq.* (2024) 124252, <https://doi.org/10.1016/j.ijbiomac.2024.129995>.

- [33] A.M. Alsuhaibani, M.S. Refat, A.M.A. Adam, M.G. El-Desouky, A.A. El-Bindary, Enhanced adsorption of ceftriaxone antibiotics from water by mesoporous copper oxide nanosphere, *Desalination Water Treat.* 281 (2023) 234–248, <https://doi.org/10.5004/dwt.2023.29135>.
- [34] R.T. Mogharbel, K. Alkhamis, R. Felaly, M.G. El-Desouky, A.A. El-Bindary, N.M. El-Metwaly, M.A. El-Bindary, Superior adsorption and removal of industrial dye from aqueous solution via magnetic silver metal-organic framework nanocomposite, *Environ. Technol.* (2023), <https://doi.org/10.1080/09593330.2023.2178331>.
- [35] G.H. Al-Hazmi, A.M.A. Adam, M.G. El-Desouky, A.A. El-Bindary, A.M. Alsuhaibani, M.S. Refat, EFFICIENT ADSORPTION OF RHODAMINE B USING A COMPOSITE OF Fe<sub>3</sub>O<sub>4</sub>@ZIF-8: synthesis, characterization, modeling analysis, statistical PHYSICS and mechanism of interaction, *Bull. Chem. Soc. Ethiop.* 37 (2023) 211–229, <https://doi.org/10.4314/BCSE.V37I1.17>.
- [36] M.G. El-Desouky, M.A.G. Khalil, M.A.M. El-Affiy, A.A. El-Bindary, M.A. El-Bindary, Effective methods for removing different types of dyes – modelling analysis statistical physics treatment and DFT calculations: a review, *Desalination Water Treat.* 280 (2022) 89–127, <https://doi.org/10.5004/dwt.2022.29029>.
- [37] A.M. Alsuhaibani, A.A. Alayyafi, L.A. Albedair, M.G. El-Desouky, A.A. El-Bindary, Efficient fabrication of a composite sponge for Cr (VI) removal via citric acid cross-linking of metal-organic framework and chitosan: adsorption isotherm, kinetic studies, and optimization using Box-Behnken design, *Materials Today Sustainability* (2024) 100732, <https://doi.org/10.1016/j.mtsust.2024.100732>.
- [38] M. Abd El-Wahab, M.G. El-Desouky, Study the effect of antioxidants on biological activity and on homopolypropylene; mechanical and physical properties, *J. Indian Chem. Soc.* 99 (2022), <https://doi.org/10.1016/j.jiics.2022.100764>.
- [39] A.U. Khan, N. Malik, B. Singh, N.H. Ansari, M. Rehman, A. Yadav, Biosynthesis, and characterization of Zinc oxide nanoparticles (ZnONPs) obtained from the extract of waste of strawberry, *Journal of Umm Al-Qura University for Applied Sciences* (2023) 2731–6734, <https://doi.org/10.1007/s43994-023-00038-5>. In press.
- [40] G.A.A. Al-Hazmi, A.A. El-Zahhar, M.G. El-Desouky, A. El-Bindary, Superior adsorption and removal of doxorubicin from aqueous solution using activated carbon via thermally treated green adsorbent: isothermal, kinetic, and thermodynamic studies. *Environmental Technology*, In press, United Kingdom, 2022, <https://doi.org/10.1080/09593330.2022.2159540>.
- [41] G.H. Al-Hazmi, M.S. Refat, M.G. El-Desouky, F.K.M. Wali, A.A. El-Bindary, Effective removal of industrial dye from aqueous solution using mesoporous nickel oxide: a complete batch system evaluation, *Desalination Water Treat.* 273 (2022) 246–260, <https://doi.org/10.5004/dwt.2022.28875>.
- [42] M.G. El-Desouky, A.A. Alayyafi, G.A. Al-Hazmi, A.A. El-Bindary, Effect of metal organic framework alginate aerogel composite sponge on adsorption of tartrazine from aqueous solutions: adsorption models, thermodynamics and optimization via Box-Behnken design, *J. Mol. Liq.* (2024) 124392, <https://doi.org/10.1016/j.molliq.2024.124392>.
- [43] S.A. Abdulrahman, A.R. Al-khawlani, Spectrophotometric quantification of amitriptyline hydrochloride in pharmaceutical tablets: method development and validation, *Journal of Umm Al-Qura University for Applied Sciences* (2024) 1–12, <https://doi.org/10.1007/s43994-024-00122-4>.
- [44] A.M. Alsuhaibani, M.S. Refat, A.A. Atta, M.G. El-Desouky, A.A. El-Bindary, Efficient adsorption and removal of tetracycline antibiotics from aqueous solutions onto nickel oxide nanoparticles via organometallic chelate, *Desalination Water Treat.* 277 (2022) 190–205, <https://doi.org/10.5004/dwt.2022.29028>.
- [45] A.M. Alqahtani, M. Mojally, A. Sayqal, B.E. Ainousah, A. Alqamash, S. Alzaharani, G. Alqurashi, O. Wawi, A. Alsharif, Determination of lead and cadmium concentration in cosmetic products in the Saudi market, *Journal of Umm Al-Qura University for Applied Sciences* (2023) 2731–6734, <https://doi.org/10.1007/s43994-023-00088-9>. In press.
- [46] M.M. Alam, New 1, 2, 4-triazole Based Eugenol Derivatives as antiCOX-2 and Anticancer Agents, *Journal of Umm Al-Qura University for Applied Sciences*, 2024, pp. 1–12, <https://doi.org/10.1007/s43994-024-00127-z>.
- [47] L. Chen, H.-F. Wang, C. Li, Q. Xu, Bimetallic metal-organic frameworks and their derivatives, *Chem. Sci.* 11 (2020) 5369–5403.
- [48] S. Abubakar, G. Shallangwa, A. Ibrahim, Syntheses and Determination of Activities of Some Metal (II) Complexes with Derivatives of a Novel Vanillin–Tryptophan Schiff Base Ligand, *Journal of Umm Al-Qura University for Applied Sciences*, 2024, pp. 1–11, <https://doi.org/10.1007/s43994-024-00129-x>.
- [49] A. Mechoor, S. Berchmans, G. Venkatachalam, Bimetallic Cu–Zn zeolitic imidazolate frameworks as peroxidase mimics for the detection of hydrogen peroxide: electrochemical and spectrophotometric evaluation, *ACS Omega* 8 (2023) 39636–39650, <https://doi.org/10.1021/acsomega.3c05535>.
- [50] W.A. El-Fattah, A. Guesmi, N. Ben Hamadi, M.G. El-Desouky, A. Shahat, A green synthesis of cellulose nanocrystals biosorbent for remediation of wastewater containing industrial dye, *Colloids Surf. A Physicochem. Eng. Asp.* 681 (2024), <https://doi.org/10.1016/j.colsurfa.2023.132729>.
- [51] H.M. Nassef, G.A. Al-Hazmi, A.A. Alayyafi, M.G. El-Desouky, A.A. El-Bindary, Synthesis and characterization of new composite sponge combining of Metal-Organic Framework and Chitosan for the elimination of Pb (II), Cu (II) and Cd (II) ions from aqueous solutions: batch adsorption and optimization using Box-Behnken design, *J. Mol. Liq.* (2023) 123741, <https://doi.org/10.1016/j.molliq.2023.123741>.
- [52] G.A.A. Al-Hazmi, M.A. El-Bindary, M.G. El-Desouky, A.A. El-Bindary, Efficient adsorptive removal of industrial dye from aqueous solution by synthesized zeolitic imidazolate framework-8 loaded date seed activated carbon and statistical physics modeling, *Desalination Water Treat.* 258 (2022) 85–103, <https://doi.org/10.5004/dwt.2022.28397>.
- [53] M.A. El-Bindary, M.G. El-Desouky, A.A. El-Bindary, Metal-organic frameworks encapsulated with an anticancer compound as drug delivery system: synthesis, characterization, antioxidant, anticancer, antibacterial, and molecular docking investigation, *Appl. Organomet. Chem.* 36 (2022), <https://doi.org/10.1002/aoc.6660>.
- [54] S.Y. Hashemi, M. Yegane Badi, H. Pasalari, A. Azari, H. Arfaeinia, A. Kiani, Degradation of Ceftriaxone from aquatic solution using a heterogeneous and reusable O<sub>3</sub>/UV/Fe<sub>3</sub>O<sub>4</sub>@TiO<sub>2</sub> systems: operational factors, kinetics and mineralisation, *Int. J. Environ. Anal. Chem.* 102 (2022) 6904–6920, <https://doi.org/10.1080/03067319.2020.1817909>.
- [55] A. El-Wahab, M. El-Desouky, Impact of Organic Peroxide on a Moderate Molecular Weight Homo-Polypropylene Vis Breaking, and Mechanism of Interaction, *Main Group Chemistry*, 2023, pp. 1–12, <https://doi.org/10.3233/MGC-230024>. In press.
- [56] H.H. Alsharif, N.M. Alatawi, A.M. Al-bonayan, S.H. Alrefae, F.A. Saad, M.G. El-Desouky, A.A. El-Bindary, Adsorption of Azorubine E122 dye via Na-mordenite with tryptophan composite: batch adsorption, Box–Behnken design optimisation and antibacterial activity, *Environ. Technol.* (2023), <https://doi.org/10.1080/09593330.2023.2219399> (United Kingdom), In press.
- [57] S.D. Al-Qahtani, M. Alhasani, N. Alkhatami, K.A. Abu Al-Ola, K. Alkhamis, M.G. El-Desouky, A.A. El-Bindary, Effective levofloxacin adsorption and removal from aqueous solution onto tea waste biochar; synthesis, characterization, adsorption studies, and optimization by Box–Behnken design and its antibacterial activity, *Environ. Technol.* (2023), <https://doi.org/10.1080/09593330.2023.2283409> (United Kingdom), In press.
- [58] S. Ibrahim, Review on synthesis of novel carbonyl derivatives of biological macromolecules by oxidation of polysaccharides with permanganate ion in alkaline media, *Journal of Umm Al-Qura University for Applied Sciences* (2024) 1–19, <https://doi.org/10.1007/s43994-023-00098-7>.
- [59] A.A. Alluhaybi, A. Alharbi, K.F. Alshammari, M.G. El-Desouky, Efficient adsorption and removal of the herbicide 2,4-dichlorophenylacetic acid from aqueous solutions using MIL-88(Fe)-NH<sub>2</sub>, *ACS Omega* 8 (2023) 40775–40784, <https://doi.org/10.1021/acsomega.3c05818>.
- [60] N.M. El-Metwaly, H.A. Katouah, M.G. El-Desouky, A.A. El-Bindary, M.A. El-Bindary, Fabricating of Fe<sub>3</sub>O<sub>4</sub>@Ag-MOF nanocomposite and evaluating its adsorption activity for removal of doxorubicin, *Journal of Environmental Science and Health - Part A Toxic/Hazardous Substances and Environmental Engineering* 57 (2022) 1099–1115, <https://doi.org/10.1080/10934529.2022.2156230>.
- [61] G.A.A. Al-Hazmi, A.A. El-Zahhar, M.G. El-Desouky, M.A. El-Bindary, A.A. El-Bindary, Efficiency of Fe<sub>3</sub>O<sub>4</sub>@ZIF-8 for the removal of Doxorubicin from aqueous solutions: equilibrium, kinetics and thermodynamic studies, *Environ. Technol.* 45 (2024) 731–750, <https://doi.org/10.1080/09593330.2022.2121181>.
- [62] H.M.F. Freundlich, Over the adsorption in solution, *J. Phys. Chem.* 57 (1906) 385–471, <https://doi.org/10.1515/zpch-1907-5723>.
- [63] M. Dubinin, The equation of the characteristic curve of activated charcoal, *Proc. Acad. Sci. USSR Phys. Chem. Sect.* 55 (1947) 327–329.
- [64] V.P.M.I. Tempkin, Kinetics of ammonia synthesis on promoted iron catalyst, *Acta Phys. Chim. USSR* 12 (1940) 327–356, <https://doi.org/10.1016/j.jtice.2019.10.006>.
- [65] W.S. Wan Ngah, N.F.M. Ariff, M.A.K.M. Hanafiah, Preparation, characterization, and environmental application of crosslinked chitosan-coated bentonite for tartrazine adsorption from aqueous solutions, *Water Air Soil Pollut.* 206 (2010) 225–236, <https://doi.org/10.1007/s11270-009-0098-5>.
- [66] O. Redlich, D.L. Peterson, A useful adsorption isotherm, *J. Phys. Chem.* 63 (1959) 1024, <https://doi.org/10.1021/J150576A611>, 1024.

- [67] I. Langmuir, The constitution and fundamental properties of solids and liquids. Part I. Solids, *J. Am. Chem. Soc.* 38 (1916) 2221–2295, [https://doi.org/10.1016/S0016-0032\(17\)90938-X](https://doi.org/10.1016/S0016-0032(17)90938-X).
- [68] H. Alessa, N. Algethami, Up-to-date Studies Regarding the Determination of Sertraline by Different Analytical Methods, *Journal of Umm Al-Qura University for Applied Sciences*, 2024, pp. 1–16, <https://doi.org/10.1007/s43994-023-00112-y>.
- [69] S.K. Lagergren, About the theory of so-called adsorption of soluble substances, *Sven. Vetenskapsakad. Handlingar* 24 (1898) 1–39.
- [70] Y.-S. Ho, G. McKay, Pseudo-second order model for sorption processes, *J Process biochemistry* 34 (1999) 451–465, [https://doi.org/10.1016/S0032-9592\(98\)00112-5](https://doi.org/10.1016/S0032-9592(98)00112-5).
- [71] W.J. Weber Jr., J.C. Morris, Kinetics of adsorption on carbon from solution, *J. Sanit. Eng. Div.* 89 (1963) 31–59, <https://doi.org/10.1061/JSEDAI.0000430>.
- [72] M. Vlad, E. Segal, A kinetic analysis of Langmuir model for adsorption within the framework of Jovanovic theory; a generalization of the Jovanovic isotherm, *J. Surf. Sci.* 79 (1979) 608–616, [https://doi.org/10.1016/0039-6028\(79\)90308-X](https://doi.org/10.1016/0039-6028(79)90308-X).
- [73] G.H. Al-Hazmi, M.G. El-Desouky, A.A. El-Bindary, Synthesis, characterization and microstructural evaluation of zno nanoparticles by william-hall and size-strain plot methods, *Bull. Chem. Soc. Ethiop.* 36 (2022) 815–829, <https://doi.org/10.4314/bcse.v36i4.8>.
- [74] A.S. Al-Wasidi, I.I.S. AlZahrani, A.M. Naglah, M.G. El-Desouky, M.A. Khalil, A.A. El-Bindary, M.A. El-Bindary, Effective removal of methylene blue from aqueous solution using metal-organic framework; modelling analysis, statistical physics treatment and DFT calculations, *ChemistrySelect* 6 (2021) 11431–11447, <https://doi.org/10.1002/slct.202102330>.
- [75] M.G. El-Desouky, M.A. El-Bindary, A.A. El-Bindary, Effective adsorptive removal of anionic dyes from aqueous solution, *Vietnam Journal of Chemistry* 59 (2021) 341–361, <https://doi.org/10.1002/vjch.202000184>.
- [76] M.G. El-Desouky, A.A. El-Bindary, Magnetic metal-organic framework (Fe<sub>3</sub>O<sub>4</sub>@ZIF-8) nanocomposites for adsorption of anionic dyes from wastewater. *Inorganic and Nano-Metal Chemistry*, 2021, <https://doi.org/10.1080/24701556.2021.2007131>. In press.
- [77] M.G. El-Desouky, N. Hassan, A. Shahat, A. El-Didamony, A.A. El-Bindary, Synthesis and characterization of porous magnetite nanosphere iron oxide as a novel adsorbent of anionic dyes removal from aqueous solution, *Biointerface Research in Applied Chemistry* 11 (2021) 13377–13401, <https://doi.org/10.33263/BRIAC115.1337713401>.
- [78] A. Almahri, K.S. Abou-Melha, H.A. Katouah, A.M. Al-bonayan, F.A. Saad, M.G. El-Desouky, A.A. El-Bindary, Adsorption and removal of the harmful pesticide 2,4-dichlorophenylacetic acid from an aqueous environment via coffee waste biochar: synthesis, characterization, adsorption study and optimization via Box-Behnken design, *J. Mol. Struct.* (2023) 1293, <https://doi.org/10.1016/j.molstruc.2023.136238>.